Key Points:
- There were marked decreases in the level of aerosols, SO_2, and NO_2 over COVID epicenters and subregion during the periods of lockdown
- During the same period, there was a slight increase in ozone and CO over most of the COVID epicenters and the subregion
- There was a shift in the size distribution of prevailing aerosol cluster toward the coarse fractions

Correspondence to:
O. G. Fawole,
olusegun.fawole@port.ac.uk

Author Contributions:
Conceptualization: Olusegun G. Fawole, Najib Yusuf, Lukman A. Sunmonu, Aderonke Obafaye, Dauda K. Audu, Abdoulaye Deme, Habib Senghor
Data curation: Olusegun G. Fawole, Lukman A. Sunmonu, Aderonke Obafaye, Dauda K. Audu, Loretta Onuorah, Christiana F. Olusegun
Formal analysis: Olusegun G. Fawole, Christiana F. Olusegun
Investigation: Olusegun G. Fawole

Impacts of COVID-19 Restrictions on Regional and Local Air Quality Across Selected West African Cities

Olusegun G. Fawole[1,2] , Najib Yusuf[3] , Lukman A. Sunmonu[2] , Aderonke Obafaye[3], Dauda K. Audu[3] , Loretta Onuorah[4] , Christiana F. Olusegun[3] , Abdoulaye Deme[5], and Habib Senghor[6]

[1]School of the Environment, Geography and Geosciences, University of Portsmouth, Portsmouth, UK, [2]Department of Physics and Engineering Physics, Obafemi Awolowo University, Ile-Ife, Nigeria, [3]Centre for Atmospheric Research (CAR), National Space Research and Development Agency, Kogi State University, Anyigba Campus, Abuja, Nigeria, [4]Department of Physical and Geosciences, Godfrey Okoye University, Enugu, Nigeria, [5]UFR Sciences Appliquees et Technologie (SAT), Universite Gaston Berger, Saint-Louis, Senegal, [6]Senegalese National Agency of Civil Aviation and Meteorology (ANACIM), Dakar, Senegal

Abstract The emergence of COVID-19 brought with it panic and a sense of urgency causing governments to impose strict restrictions on human activities and vehicular movements. With anthropogenic emissions, especially waste management (domestic and municipal), traffic, and industrial activities, said to be a significant contributor to ambient air pollution, this study assessed the impacts of the imposed restrictions on the concentrations and size distribution of atmospheric aerosols and concentration of gaseous pollutants over West African subregion and seven major COVID-19 epicenters in the subregion. Satellite retrievals and reanalysis data sets were used to study the impact of the restrictions on Aerosol Optical Depth (AOD) and atmospheric concentrations NO_2, SO_2, CO, and O_3. The anomalies were computed for 2020 relative to 2017–2019 (the reference years). In 2020 relative to the reference years, for area-averaged AOD levels, there was a consequential mean percentage change between $-6.7\% \pm 21.0\%$ and $19.2\% \pm 27.9\%$ in the epicenters and $-10.1\% \pm 15.4\%$ over the subregion. The levels of NO_2 and SO_2 also reduced substantially at the epicenters, especially during the periods when the restrictions were highly enforced. However, the atmospheric levels of CO and ozone increased slightly in 2020 compared to the reference years. This study shows that "a one cap fits all" policy cannot reduced the level of air pollutants and that traffic and industrial processes are not the predominant sources of CO in major cities in the subregion.

Plain Language Summary The emergence of COVID-19 in December 2020 caused national and regional governments to introduce lockdown and restrict the movement of vehicles and human. There was also a significant reduction or total stoppage of industrial activities. This study, in the absence of reliable long-term ground-based measurement of ambient air pollutants, used observations from satellites and reanalysis data sets to investigate the level of air pollutants in the airshed of seven (7) major COVID-19 epicenters in the West African subregion and also over the entire subregion during the periods of lockdown. The level of pollutants during the pandemic in 2020 was compared against the mean of the three preceding years (2017–2019) to calculate the anomalies. The level of aerosol aerosol optical depth, SO_2, and NO_2 reduced substantially in 2020 compared to the reference years. However, the atmospheric levels of ozone and CO increased slightly in 2020 as against the reference years. The slight increase in CO levels could be attributed to local burning of domestic waste and biomass burning. There was a shift in the size distribution of atmospheric aerosols cluster toward the coarse fraction.

1. Introduction

In late December 2019, an acute respiratory disease was discovered in a cluster of humans in the indoor Huanan seafood wholesale market in Wuhan, Hubei province, China (Li et al., 2020). Symptoms of the disease include fever, fatigue, cough, and acute dyspnea (Fu et al., 2020; Rodriguez-Morales et al., 2020; Spychalski et al., 2020). The disease, later linked to the family of coronaviruses, was named COVID-19 by the World Health Organization (WHO). COVID-19 was declared a Public Health Emergency of International Concern on 30 January 2020 and a pandemic on 11 March 2020 (Eurosurveillance Editorial Team, 2020; Ntoumi & Velavan, 2021; Schwartz & Graham, 2020). Movement of people, especially tourists, during the Chinese New Year celebration in December

Methodology: Olusegun G. Fawole, Najib Yusuf, Lukman A. Sunmonu, Abdoulaye Deme, Habib Senghor
Project Administration: Najib Yusuf
Supervision: Olusegun G. Fawole
Visualization: Olusegun G. Fawole, Christiana F. Olusegun, Abdoulaye Deme, Habib Senghor
Writing – original draft: Olusegun G. Fawole, Najib Yusuf, Lukman A. Sunmonu, Aderonke Obafaye, Dauda K. Audu, Loretta Onuorah, Christiana F. Olusegun, Abdoulaye Deme, Habib Senghor
Writing – review & editing: Olusegun G. Fawole, Najib Yusuf, Lukman A. Sunmonu

2019 was partly responsible for the fast spread of the disease within and outside China (Bogoch et al., 2020; Chen & Yu, 2020; Yu & Chen, 2020).

Despite its widespread in Europe and Asia, prompting the restriction of movements (human and vehicular) and the imposition of local, national, and regional lockdowns and border controls by government at various levels, the epidemic did not become prevalent in Africa until mid-March 2020. While Egypt recorded the first case of the virus on 14 February, twenty-seven (27) other African countries recorded their first cases between 13 and 20 March, 2020, about 30 days after Egypt recorded its first case of the virus on the continent. The first case of the disease was recorded in the seven (7) West African countries covered in this study—Nigeria, Senegal, Burkina Faso, Ghana, Côte D'Ivoire, Cameroon, and Mali—between 28 February and 26 March 2020. On the African continent, with 54 countries, it took 90 days for the number of confirmed cases to reach 100 000 but just 19 days to double the number of confirmed cases and another 12 days to reach 300 000 (Wadvalla, 2020). As of 12 October 2021, the cumulative number of cases and fatalities on the continent has risen to 6,087,812 and 121,597, respectively (data accessed from https://covid19.who.int on 12 October 2021). The first official COVID-19 death in Africa was announced on 8 March 2020, in Egypt.

From the aforementioned, it is clear that the spread of the pandemic to Africa started much later than other parts of the globe. In addition, the rate of infection and fatality on the African continent is much lower than projections made by international bodies such as the WHO and the Bill and Melinda Gates Foundation (Njenga et al., 2020). The lower incidences and fatalities of COVID-19 experienced in Africa have been attributed to a number of factors including younger population, fewer percentage of the population living with comorbidities, and life expectancy (Lawal, 2021). Despite the relatively low incidences and fatalities in Africa, to curb the spread and resulting deaths, the governments in most African countries were forced to resort to national or regional lockdowns and restricted human and vehicular movement. These were done so as not to put the already strained and underfunded healthcare systems in most African countries under pressure, which could result in increased fatalities. During the first and second waves of the pandemic in 2020, the periods of the lockdown run for weeks and even months at a stretch in many African countries and occurred at different times and with overlaps. Some West African countries eased the restrictions briefly but had to reimpose them after experiencing significant spikes in the number of incidences and fatalities. There were also occasions when the restrictions were temporarily eased for a day or two to allow people to restock their food and other essentials. Table 1 gives a breakdown of the periods of restriction in the seven West African countries considered in this study.

In most developing economies around the world, especially in low- and middle-income countries (LMICs), air quality (AQ) is at its lowest ebb because of the rapid economic and population growth and industrialization efforts experienced in most cities in LMICs are not backed up with sustainable management of the environment. The source of air pollutants in most West African cities is a combination of anthropogenic and natural, with pollutants from anthropogenic sources being the most dominant in urban airsheds (Dominutti et al., 2019; Liousse et al., 2014; Marticorena et al., 2010; Naidja et al., 2018). In the West African subregion, most emissions from natural sources, for example, desert dust and biomass burning, are often seasonal or episodic (Bauer et al., 2019). Anthropogenic sources of emissions include industrial processes, traffic, power generation, construction works, road dust resuspension, domestic cooking, and waste burning (Fayiga et al., 2018; Hoesly et al., 2018). Human activities and traffic are ubiquitous and often times uncontrolled and unmonitored in most cities in the subregion where more than 80% of automobiles on the roads are secondhand used vehicles imported from Europe and the United States and waste (domestic and municipal) burning is carried out indiscriminately.

Globally, COVID-19 pandemic led to unprecedented restriction of movements that brought about a drastic reduction of global and local travels due to border closures and closure of schools and businesses, including stoppage or massive reduction of industrial activities. As a result of these restrictions, many countries observed clear blue skies for the very first time in decades. Several studies in different regions of the world—Srivastava et al. (2021) (India), Menut et al. (2020) (western Europe), Filonchyk et al. (2021) (Poland), Matthias et al. (2021) (central Europe), Stratoulias and Nuthammachot (2020) (Thailand), Fuwape et al. (2021) (Nigeria), and Archer et al. (2020) (USA), just to mention a few—have reported various levels of improvement in AQ during the various lockdown periods, which lasted for months in some countries, especially in epicenters and neighboring cities.

Using AQ and meteorological data from ground-based and satellite platforms, studies from several countries and regions of the world have reported varying degrees of reduction in air pollution and improved Air Quality Indices,

Table 1
Breakdown of the Location of Epicenters and Restriction Periods

Country	Epicenter	Land area (km²)	Coordinate	Period of restrictions in 2020 (approx.)[a]
Nigeria	Lagos	3,577	6.3–7°N	March 30 -mid May
			2.7–4.3°E	Mid July -September
Senegal	Touba	97.2	14.6–14.8°N	March—June
			17.5–17.3°W	August—October
Ghana	Accra & Ashanti region	24,389	5.9–7.6°N	March—July
			2.5–0.2°W	August—September
Mali	Bamako	245	12.5–12.7°N	March—May
			8.1–7.9°W	July—September
Côte D'Ivoire	Abidjan	2,119	5.3–5.5°N	March—June
			4.1–3.9°W	August—September
Burkina Faso	Kadiogo province	2,805	12–12.7°N	March—April
			1.8–1.1°W	August
Cameroun	Center region	68,953	3.2–6.2°N	March—June
			10.2–13.2°E	July—August

[a]The periods of restrictions were estimated from https://graphics.reuters.com/world-coronavirustracker-and-maps/.

especially in COVID-19 epicenters. Serious dearth of long-term AQ data from ground-based stations has greatly impacted AQ studies in most African countries. As such, studies on long-term trends and variability of atmospheric pollutants in this region have resorted to the use of data from remote sensing (e.g., AERONET, (Boiyo et al., 2017; Fawole et al., 2016; Yusuf et al., 2021)), reanalysis (e.g., MERRA-2, (Diop et al., 2018; Veselovskii et al., 2018)), and satellite platforms (e.g., OMI; (Lourens et al., 2012; Marais et al., 2012)).

Using aerosol optical depth (AOD), Angstrom Exponent (AE), and single scattering albedo (SSA), the study investigates the anomalies in the loading, size distribution, and optical properties of dominant aerosols during the pandemic. The anomalies were estimated as the atmospheric concentrations of the pollutants in 2020 relative to the mean of the three preceding years (2017–2019), herein referred to as the "reference years." To the best of the authors' knowledge, this is the first study to attempt an assessment of the anomalies of gaseous pollutant and aerosol loading as well as size distribution in the subregion during the pandemic. This study brings into context the possible impact of mitigation strategies and other government policies to improve AQ in the study regions. It also shows the possible limitations that could impede the use of satellite retrievals for AQ monitoring in the subregion, especially for the analyses of daily mean AQ levels.

In this study, perceived anomalies in the atmospheric concentrations of four gaseous pollutants (NO_2, SO_2, O_3, and CO) and loading of atmospheric aerosol in 2020 were assessed and quantified in relation to historical mean (2017–2019). The authors hypothesized that (a) there is a marked reduction in gaseous air pollutants in the West African subregion brought about by months of limited human activities and restrictions of human and vehicular movements due to the COVID-19 pandemic and (b) there is a reduction in the loading of atmospheric aerosol and a shift in the pattern of the size distribution of aerosol toward coarser aerosol cluster. The latter part of the second hypothesis is premised on the fact that most human activities such as traffic and industrial processes which were brought almost to a halt during the lockdown are the predominant sources of fine aerosol clusters in the atmosphere in most cities of the world, the epicenters not an exception. The study area covers seven (7) West African countries with higher COVID-19 incidences and fatalities during the first and second waves.

2. Material and Methods

2.1. Study Area

The study area covers the seven epicenters and lies between 0°S—22°N and 16°W—12°E. The epicenters were selected because of the relatively high number of COVID incidences and fatalities, level of compliance/effectiveness,
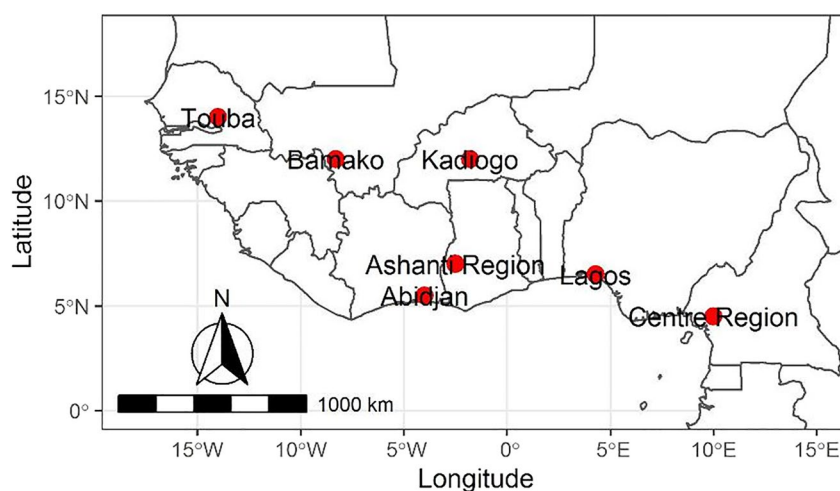
Figure 1. Map showing the subregion and location of the seven (7) epicenters.

and length of restrictions and lockdown periods. Table 1 shows, among other information, the coordinates of the epicenter in the selected countries and periods of restrictions. See Figure 1 for a map of the subregion and the selected epicenters.

2.2. Government Policies, Lockdowns, and Restrictions

The seven (7) countries considered in this study implemented various closures and restrictions of movement at different periods during the first and second waves of the pandemic between March and December 2020. The period of restrictions overlapped in most of the countries and the level of compliance varied. There were periods when the restrictions were relaxed in some part of the regions for a couple of days to a week before being reimposed. Table 1 gives a breakdown of the periods of restrictions and lockdowns. Only essential services (health care and security outfits) were allowed to run unhindered during the period of restrictions. These restrictions brought almost a halt to human activities and traffic flow, especially in the epicenters where the restrictions on travels and workplaces were more effective and prolonged. As such, the comparisons intended in this study will be at the finer level of the epicenters in addition to the regional levels.

2.3. Air Quality Data

The unavailability of reliable long-term ground-based AQ and meteorology data in the study area is a well-known fact to the scientific community worldwide. As such, all the data acquired and processed for the intended analyses undertaken in this study are from satellite retrievals, models, and remotely sensed data sources. All the data, aerosol and gaseous pollutant, were averaged to monthly values for ease of comparison of the data sets included in the analyses.

2.3.1. Aerosol Parameters

Three aerosol parameters—AOD, AE, and SSA—were analyzed to investigate the impact of the periods of restrictions and lockdowns during the COVID-19 pandemic on the loading, size distribution, and absorption property of prevailing atmospheric aerosol over West Africa. See Table 2 for details of the aerosol parameters included in these analyses.

2.3.1.1. Aerosol Optical Depth (AOD)

AOD is a measure of the extinction of incoming solar radiation by atmospheric aerosol. It quantifies the fraction of light prevented from reaching the Earth's surface by atmospheric aerosols. AOD is one of the fundamental optical parameters and a key parameter for the evaluation of aerosol content in atmosphere and air pollution

Table 2
Source and Specifications of Pollutants' Data Sets Included in This Study

Pollutant	Source	Temporal resolution	Spatial resolution	Unit
SO_2 (surface mass concentration)	MERRA-2	Hourly	$0.5° \times 0.625°$	kg/m^3
Ozone (total column)	OMI	Daily	$0.25° \times 0.25°$	Dobson
CO (column burden)	MERRA-2	Monthly	$0.5° \times 0.625°$	kg/m^2
NO_2 (total column) 30% cloud screened	OMI	Daily	$0.25° \times 0.25°$	$1/cm^2$
Aerosol (AOD) 550 nm	MERRA-2	Monthly	$0.5° \times 0.625°$	-
Aerosol (AOD) 550 nm	MODIS-Terra (combined dark target and deep blue)	Daily	$1° \times 1°$	-
Total angstrom aerosol parameter	MERRA-2	Hourly	$0.5° \times 0.625°$	-
Aerosol single scattering albedo (500 nm)	OMI	Daily	$1° \times 1°$	-

level. While an AOD value of <0.1 indicates a clean atmosphere, a value >0.5 indicates a hazy and aerosol laden atmosphere. AOD data at 550 nm from both MERRA-2 reanalysis and Moderate Resolution Imaging Spectroradiometer (MODIS)-Terra (combined dark target and deep blue) were used to assess the variation in aerosol loading.

MERRA data sets are managed by NASA's Global Modeling and Assimilation Office (GMAO). GMAO aimed to place historical observations from NASA's Earth Observing System satellites into the Goddard Earth Observing System (GEOS) atmospheric modeling and data assimilation system (Rienecker et al., 2011). MERRA-2, the 2nd version of MERRA, is the latest generation of the reanalysis, which addresses the limitations of the 1st version with the updated Earth system model of GEOS, version 5. MERRA-2 is the first long-term global reanalysis to assimilate space-based observations of aerosols and represent their interactions with other physical processes in the climate system.

Although the analyses of the variability of AOD over the subregion and epicenters were done with MERRA-2 reanalysis AOD parameter, MODIS AOD was used to validate MERRA-2 AOD. MODIS AOD (550 nm) obtained fromMODIS (Terra) Collection 6.1 aerosol products with the use of combined dark target and deep blue algorithm was used for the validation. Spatial resolution of the radiometer at this wavelength is 1 × 1 for the investigation of large areas and a spatial resolution of 3 km for the investigation of aerosols within urban agglomerations.

2.3.1.2. Single Scattering Albedo (SSA)

SSA relates the ratio of scattering to the extinction coefficient. It depends on particle compositions and volume size distribution in the atmosphere. Although, it is an aerosol optical parameter that is more significant in determining the aerosol radiative effect, SSA is also an important parameter in AQ studies. As the size distribution and composition of the aerosol cluster play significant roles in the determination of SSA values, SSA values can be used to infer the nature, type, and sources of aerosol particles. In the Gangetic-Himalayan region, Manoharan et al. (2014) found that coarser particle matter (PM) are about 30% more absorbing than finer PM. The study also show that under clear-sky conditions, coarser PM account for >40% of total aerosol forcing. Values of SSA range from 0 for a purely absorbing aerosol to 1 for a purely scattering aerosol. And, the major absorbing aerosol species are black carbon (BC) (Bond et al., 2013), mineral dust (Claquin et al., 1999), and organic aerosols such as brown carbon (Andreae & Gelencsér, 2006).

SSA retrieved by the near-UV two-channel algorithm (OMAERUV) applied to the Aura/Ozone Monitoring Instrument (OMI) measurements was analyzed to assess the impact of restrictions occasioned by the pandemic on optical properties of atmospheric aerosols. SSA data were obtained as time series, area-averaged at wavelength 500 nm, level 3, version 3 data with $1° \times 1°$ spatial resolution (OMAERUVd) from similar satellite OMI but at daily scales and then averaged into monthly mean. Complete SSA data are available for only three of the seven epicenters. The analyses of the SSA data were carried out over the West African subregion alone because SSA data were available for only three of the seven epicenters. The anomalies in SSA between 2017 and 2019 and 2020 were computed to assess the changes in absorption properties of aerosol due to restrictions during the

COVID-19 pandemic. Understanding the optical property on dominant aerosol clusters is of great importance as these properties determine their interaction with incoming shortwave and outgoing longwave radiation.

2.3.1.3. Angstrom Exponent (AE)

AE is an operationally robust optical parameter that contains information on the size distribution of all optically active aerosols in the field of view of a sun photometer (O'Neill et al., 2001). Analysis of the AE over the epicenters is important as the characterization of the particle size distribution will enhance the drawing of inferences about the impact of restrictions due to the COVID-19 pandemic on dominant aerosol particles in the atmosphere in 2020. Thirty-minute averages of AE are clustered into bins based on the aerosol modes. One constant value of AE is not a good threshold to classify the aerosol types. However, $AE \leq 1.0$ and $AE > 1.0$ are typically representative of coarse-mode and fine-mode-dominated aerosol clusters, respectively (Kaufman, 1993). The closer the value of AE is to zero, the coarser the aerosol particle.

2.3.2. Gaseous Air Pollutant

Anthropogenic pollution is estimated using the atmospheric loading of NO_2, CO, SO_2, and O_3 averaged over the region and on a finer scale, the epicenters. Details of the sources, units, and spatial resolution of the data are given in Table 2. OMI is an ultraviolet/visible nadir solar backscatter spectrometer that makes daily measurement of Earth radiance and solar irradiance from 270 to 500 nm with spectral resolution of 0.5 nm. It provides nearly global coverage in one day, with a spatial resolution of 13×24 km. Atmospheric gases measured are O_3, NO_2, SO_2, HCHO, BrO, and OClO. In addition, OMI measures aerosol characteristics, cloud top heights, and cloud coverage (Jethva et al., 2014; Levelt et al., 2006). With its high spatial resolution and daily global coverage, OMI promises highly interesting scientific results that could enhance our understanding of stratospheric and tropospheric chemistry and climate change (Balis et al., 2007).

2.3.2.1. Nitrogen Dioxide (NO_2)

NO_2 is an important chemical species in both the stratosphere, where it plays a key role in ozone chemistry, and the troposphere, where it is a precursor to ozone production. NO_2 is an anthropogenic pollutant emitted from combustion processes, traffic, and industrial activities. We use level-3 daily global gridded ($0.25° \times 0.25°$) nitrogen dioxide product (OMNO2d). OMNO2d is produced for all atmospheric conditions in the total column NO_2 and the total tropospheric column NO_2, and for sky conditions where cloud fraction is $<30\%$ (Lamsal et al., 2021).

2.3.2.2. Ozone (O_3)

Ozone is a secondary pollutant as such its atmospheric concentration relies on prevailing meteorology and concentration of its precursors—NO_X (NO + NO_2), volatile organic compounds (VOCs), and CO. Majority of tropospheric ozone is formed when NO_X, VOCs, and CO react in the presence of sunlight. The prominent sources of these precursors are biomass burning, traffic emission, industrial activities, lightening NO_X, and stratospheric injection (Levelt et al., 2006).

Two satellite data products are available for total column ozone—TOMS and differential optical absorption spectroscopy (DOAS). OMI total column ozone data are retrieved using both the TOMS V8 retrieval algorithm developed by NASA (Balis et al., 2007) and a DOAS technique developed by Royal Netherlands Meteorological Institute (KNMI) (Veefkind et al., 2006). Both algorithms provide OMI ozone data of the same quality as TOMS ozone data in order to ensure continuity of ozone trends detected to date. Comparing total ozone products from TOMS V7 retrieval with thirty ground-based station, McPeters and Labow (1996) found that the TOMS ozone data compare within $\pm 1\%$ of ground-based measurements.

2.3.2.3. Carbon Monoxide (CO)

The atmospheric sources of CO, an odorless, tasteless, and colorless gas, are combustion of fossil fuel, biomass burning, and oxidation of methane and biogenic hydrocarbons (Holloway et al., 2000). Monthly mean column burden of CO from MERRA-2 was used to assess the atmospheric levels of CO in this study. MERRA project focuses on historical climate analyses for both weather and climate timescales. This reanalysis covers the period from 1980 to present, continuing as an ongoing climate analysis as resources allow. Several studies, (Cao

et al. (2021); Shikwambana (2019); Shikwambana and Kganyago (2021)), have used MERRA2 products such as SO_2, BC, and CO to investigate the atmospheric concentrations of pollutants both on local and regional scales.

2.3.2.4. Sulfur Dioxide (SO_2)

SO_2 is the predominant anthropogenic sulfur-containing air pollutant emitted from the combustion of fossil fuels, which generates mainly SO_2 together with some fraction of other sulfur compounds like SO_3, H_2SO_4, and H_2S. The amount of SO_2 emitted from the combustion of a fossil fuel type depends on the sulfur content of the fuel. Mixing ratios in continental background air range from 20 ppt to 1 ppb. The lifetime of SO_2 is around 1 week on average (Seinfeld & Pandis, 2016).

Hourly averaged SO_2 surface mass concentration (M2T1NXAERV5.12.4) data were used in the analyses undertaken in this study. These were averaged to monthly values to estimate the monthly anomaly of SO_2 over the subregion and the seven epicenters.

2.4. Statistical Analyses

2.4.1. Anomalies

The monthly anomalies of the parameters are computed as the difference between the monthly values for year 2020 and monthly average of the reference years (2017–2019). The mean annual anomaly is taken as the mean of the monthly anomalies. Percentage monthly anomaly is calculated as follows:

$$\text{Monthly anomaly (\%)} = \left(\frac{\text{monthly values for 2020} - \text{average monthly values of ref. years}}{\text{monthly value for 2020}} \right) \times 100 \quad (1)$$

Anomalies for the months of January and February were excluded from the computation of the mean annual anomalies for all the pollutants because the various restrictions in all the epicenters considered started in March. Anomalies for particulates (AOD) and gaseous pollutants were first assessed and discussed over the subregion and then on the finer level of the epicenters.

2.4.2. Binning of Angstrom Exponent

To examine and classify the size distribution of atmospheric aerosol in the year 2020 in relation to the reference years, bins of the 30 min averages of AE, $AE_{470-870}$, were created. The binning was created for 2020 and the average of the reference years. For each data sets, thirty (30) bins were created for values of $AE_{470-870}$ between 0 and 2.

2.4.3. Correlation, Mean Bias Error, and Standard Deviation

Apart from anomaly, other statistical indicators used in these analyses are defined as follows:

$$r = \frac{\sum_{i=1}^{n} (x_i - \bar{x})(y_i - \bar{y})}{\sqrt{\left(\sum_{i=1}^{n} (x_i - \bar{x})^2 \right) \left(\sum_{i=1}^{n} (y_i - \bar{y})^2 \right)}} \quad (2)$$

$$SD = \sqrt{\frac{\sum (x - \bar{x})^2}{n - 1}} \quad (3)$$

$$MBE = \frac{1}{n} \sum_{i=1}^{n} (x_i - y_i) \quad (4)$$

where r is the correlation coefficient, SD is the standard deviation, MBE is the mean bias error, n is the number of terms, x and y are the two pairs of data, and $\bar{x}$ and $\bar{y}$ are the mean of x and y.

3. Results and Discussion

The comparison of the various pollutants in 2020 relative to the average of reference years was done at both the regional (West Africa) and epicenter levels. The impact of the lockdowns and restrictions on the atmospheric

Table 3
Statistical Analyses of the Comparison of Moderate Resolution Imaging Spectroradiometer (MODIS) and MERRA2 Aerosol Optical Depth Products

Location	r	MBE	Abs. bias (%)
Abidjan	0.94	0.093	21.2
Accra and Ashanti region	0.91	0.002	2.7
Bamako	0.76	−0.025	28.0
Center region	-	-	
Kadiogo	0.87	0.019	3.5
Lagos	0.96	0.090	18.0
Touba	0.98	0.038	14.1
Regional (West Africa)	0.91	0.063	13.2

concentration of each pollutant at both local and regional levels was subsequently discussed on the background that the restrictions were more effective in some epicenters than others.

3.1. Aerosol Parameters

3.1.1. AOD

Due to paucity of ground-based measurement, MODIS AOD data were used to validate and assess the representativeness, relative consistency, and accuracy of the MERRA2 AOD parameter used in this study. Area-averaged daily values of combined dark target and deep blue AOD (550 nm) for land and sea are used for the validation. MERRA2 AOD parameters are used for the intended analyses in this study because MODIS aerosol parameter is not available for Center Region (Cameroon), one of the seven epicenters included in this study.

Table 3 gives the statistical description of the comparison of the two AOD data sets over the West Africa region and at the epicenters. Monthly average AOD for the four years, 2017–2020, considered in this study are included in the statistical analyses of the comparison. The comparison of AOD (550 nm) from MODIS Terra and MERRA-2 shows high correlation (r) levels ($0.76 \leq r \leq 0.98$) of the two data sets at the epicenters and over the subregion. The biases in the two data sets in all the epicenters but one and over the subregion fall within the range of expected bias set by MODIS over the land ($0.05 \pm 0.15 \times AOD$). The MBE and absolute bias were calculated to assess and quantify the difference between the two data sets. The two parameters which are from two different sources with very different methodologies give data sets that are highly comparable. AOD estimation by MODIS is slightly higher than that from MERRA2 reanalysis across all the epicenters and over the region except at Bamako. However, the two data are highly correlated across the epicenters and over the region. As such, MERRA2 AOD data set used in these analyses is a good representation of the aerosol loading in the study sites.

3.1.1.1. Regional AOD Anomaly

Figure 2 shows the spatial and temporal variation of the AOD anomalies over the West African subregion. The spatial plot in Figure 2a, the annual average of the anomaly over the region, shows a contrasting distribution of the anomalies over the subregion. The monthly variation of the anomaly presented in Figure 2b shows a decrease of 10%–18% in aerosol loading (AOD) during the periods of lockdown and restrictions indicated by the red boxes. These two boxes indicate the first and second waves of the pandemic in the region. The average annual anomaly of AOD in the region is −10.1% ± 15.4%. This implies that relative to the reference years, there was a marked reduction in aerosol loading in the year 2020, especially during the lockdown periods which could be attributed
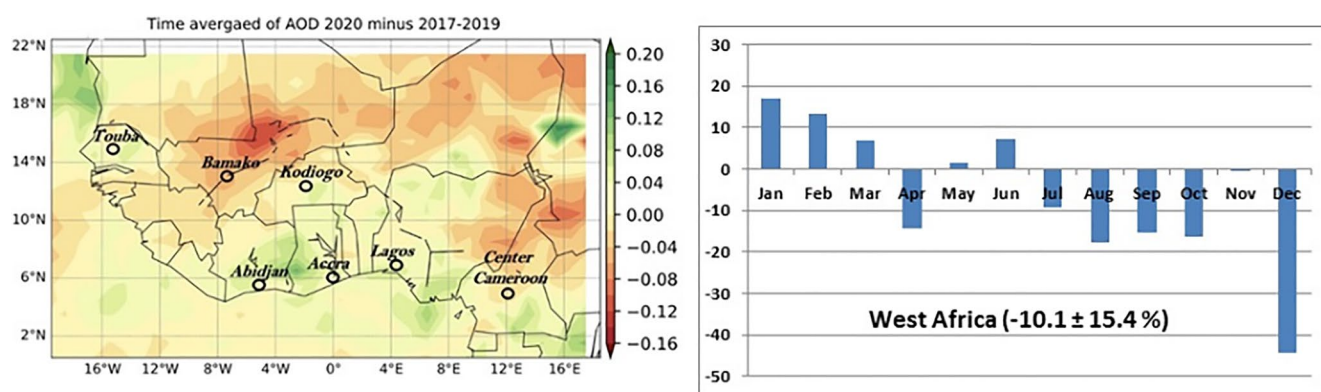
Figure 2. Variation of aerosol optical depth (AOD) anomaly over the West African sub–region (a) spatial variation and (b) temporal (monthly) variation. The red boxes show the period of restrictions during the first and second waves across the subregion. The spatial plot shows the annual average AOD over the study region containing the epicenters.
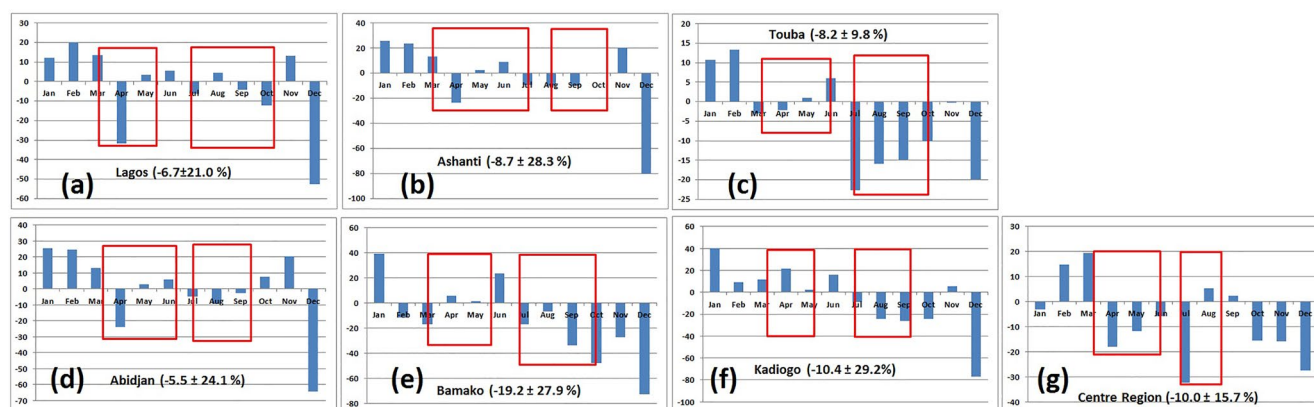
Figure 3. Temporal variation of percentage monthly anomalies of aerosol optical depth over the epicenters. The anomalies for January and February have been excluded from the estimation of the average anomalies for the subregion and the epicenters.

to reduced anthropogenic activities in 2020. In Section 3.1.1.2, the anomalies in AOD will be examined at a high resolution over the epicenters.

3.1.1.2. AOD Anomalies Over Epicenters

As presented in Table 1, there are overlaps in the period of restrictions and lockdowns across the epicenters. The effectiveness and level of compliance with the restrictions vary from one epicenter to the other. As such, varying degrees of impacts on the atmospheric aerosol loadings were quantified over the epicenters. Across the seven epicenters, there were marked consequential reductions in aerosol loading (AOD) with the most and least annual mean percentage AOD anomaly of −19.2% ± 27.9% and −5.5% ± 24.1% over Bamako and Abidjan, respectively. The percentage annual mean (±SD) anomalies in AOD over Lagos, Touba, Ashanti region, Kadiogo, and Center Region are −6.7% ± 21.0%, −8.2% ± 9.8%, −8.7% ± 28.3%, −10.4% ± 29.2%, and −10.0% ± 15.7%, respectively. The high reduction in AOD level in the month of December over the subregion and the epicenters could be attributable to the very low-key celebrations of Christmas and New Year in 2020 as the celebrations were without the usual pomp and pageantry. Figure 3 presents the temporal (monthly) variation of the percentage anomalies in AOD at the seven (7) epicenters.

3.1.2. Angstrom Exponent

The binning of 30 min averages of $AE_{470-870}$, an aerosol parameter to infer the size distribution of aerosols in a cluster, in the year 2020 and average for the reference years over the seven epicenters is presented in Figure 4. Considering the count of the coarsest particle cluster ($AE_{470-870} < 0.6$), a comparison of the two sets of data was carried out. Although at varying degrees, during the lockdown, there were more days of coarse particle dominated aerosol clusters over the epicenters. This could be attributed to the significant reduction of human activities during the period of restrictions and lockdowns. As presented in Figures 4a–4g, the total count in the red boxes representing the coarsest particle cluster are more in year 2020 compared to the average of the reference years. Table 4 presents a quantitative description of the statistics of the counts and anomalies in the bins of the coarsest aerosol cluster ($AE \leq 0.6$) shown in Figure 4. These analyses show that there were more coarse particles in the atmosphere in year 2020 than in the reference years which could invariably impact the nature of interaction between aerosol and incoming shortwave radiation, thereby affecting the Earth's energy budget. Studies have found that the radiative parameters of aerosols are strongly dependent on the size of the particles with coarse particles suggested to absorb more radiation causing more warming (Tegen & Lacis, 1996).

As hypothesized, across all the epicenters except Kadiogo (Burkina Faso), mean percentage anomaly in AE ($AE \leq 0.6$) ranges between 3% and 28% (see Table 4), indicating a dominance of coarse aerosol particles in the atmosphere in 2020 compared to the reference years. The level of compliance with the lockdown and various restrictions could be responsible for the peculiarity of the AE anomaly observed in Kadiogo.
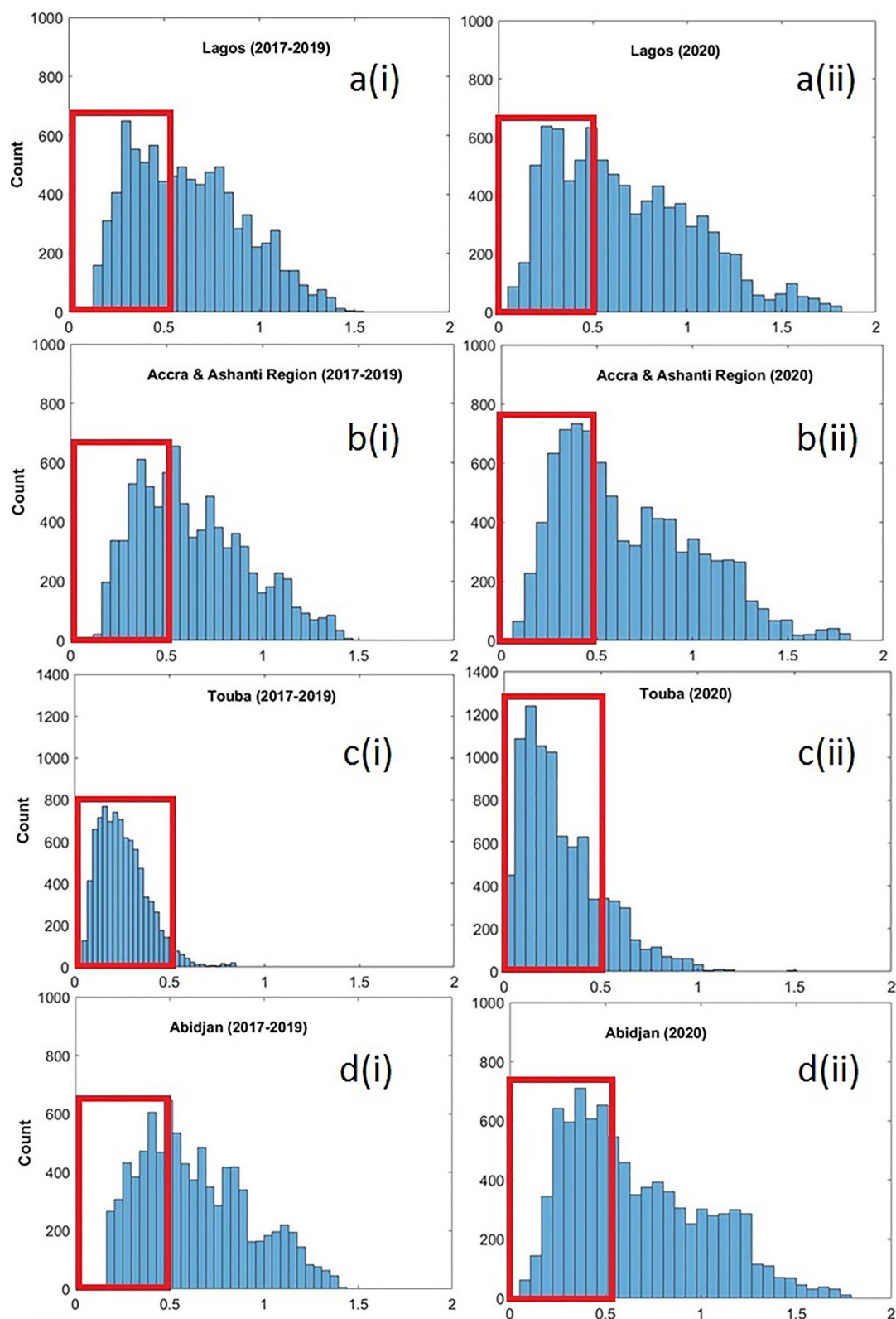
Figure 4. Histogram of the binned angstrom exponent at the epicenters with the red boxes showing the coarsest aerosol bins; (h) monthly anomaly of single scattering albedo over West Africa. a(i)–g(i) shows bins for the subregions (average of 2017–2019) and a (ii)–g(ii) shows bins for 2020.
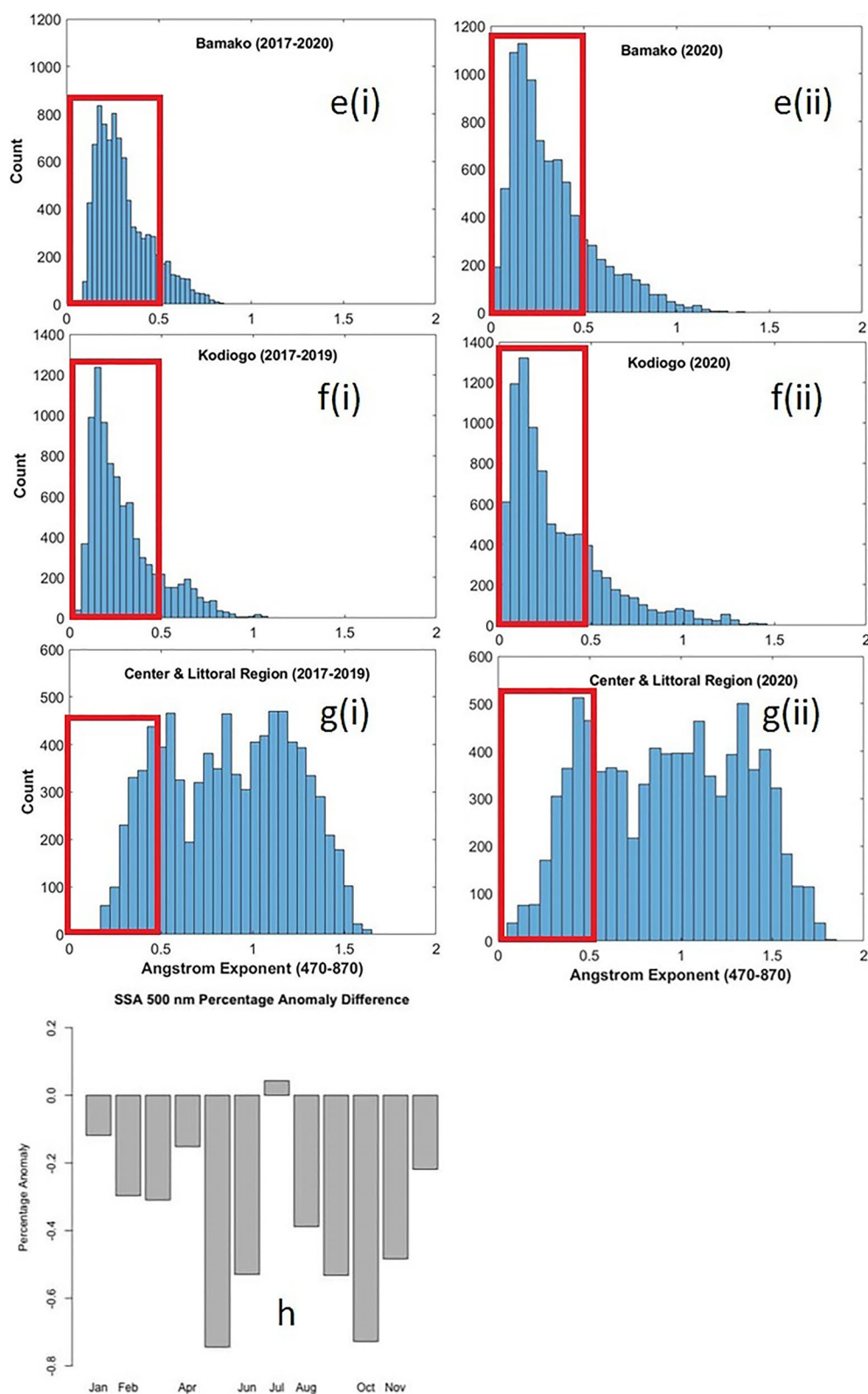
Figure 4. (Continued)

Table 4
Statistics of the Angstrom Exponent (AE) Count in the Bins and Percentage Anomaly

	AE bins	**0–0.1**	**0.1–0.2**	**0.2–0.3**	**0.3–0.4**	**0.4–0.5**	**0.5–0.6**	
Abidjan	2017–19	0	6	1,006	857	1,073	1,181	
	2020	0	207	987	1,305	607	1,200	
	Anomaly (%)	0	97.1	−1.9	34.3	−76.8	1.6	10.9
Lagos	2017–19	0	171	718	1,203	1,077	907	
	2020	0	258	1,143	1,079	1,156	995	
	Anomaly (%)	0	33.7	37.2	−11.5	6.8	8.8	15.0
Accra	2017–19	0	22	534	1,477	971	1,221	
	2020	8	294	399	1,348	1,444	1,090	
		100	92.5	−33.8	−9.6	32.8	−12.0	28.3
Bamako	2017–19	14	2,025	2,951	1,377	873	682	
	2020	229	2,734	1,694	1,275	954	810	
		93.9	25.9	−74.2	−8.0	8.5	15.8	10.3
Center Region	2017–19	0	3	161	561	782	861	
	2020	0	114	247	306	876	821	
		0	97.4	34.8	−83.3	10.7	−4.9	10.9
Kadiogo	2017–19	406	2,225	2,423	1,513	779	517	
	2020	664	2,514	1,740	957	458	899	
		38.9	11.5	−39.3	−58.1	−70.1	42.5	−12.4
Touba	2017–19	539	2,144	2,763	1,977	896	283	
	2020	606	3,379	2,076	1,213	965	670	
		11.1	36.5	−33.1	−63.0	7.2	57.8	2.7

*Note.* The bold values are AE bins (bins of Angstrom Exponent).

3.1.3. Single Scattering Albedo

The monthly anomaly of SSA (500 nm) was computed to quantify the variation in the absorption properties of dominant aerosol cluster in year 2020 relative to the reference years over the subregion. For each bin, a positive anomaly indicates that more coarse particles were in the atmosphere in 2020 than there were in the reference years. The values in the last column are the means of the anomalies of the six bins. SSA is an aerosol optical property that could be influenced to a large extent by the size distribution, nature, and source of the aerosols.

The percentage anomalies in SSA are negative in all the months except July, lying between −0.1% and −0.8%, which implies the dominance of a slightly more absorbing aerosol cluster (see Figure 4h). A small anomaly in SSA could cause significant change in aerosol radiative forcing potential depending on the amount and position of cloud cover (above or below aerosol) and surface albedo (Choi & Chung, 2014; Chung, 2012). The slightly enhanced absorbing tendency of dominant aerosol clusters in 2020 compared to the reference years could be attributed to the dominance of coarse particles in the atmosphere in 2020.

3.2. Gaseous Pollutants

Similar to the analyses of anomalies carried out for aerosols, atmospheric concentrations of four gaseous pollutants were assessed for 2020 against the reference years (2017–2019). See Section 2.3.2 for details and sources of the gaseous pollutants included in these analyses.
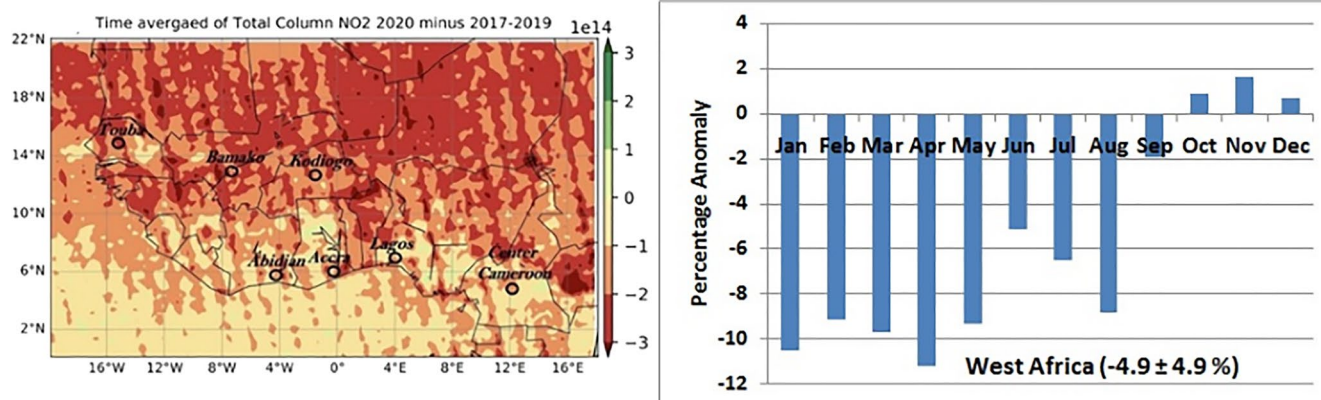
Figure 5. Variation of anomaly in NO$_2$ levels over the West African subregion (a) spatial variation and (b) temporal (monthly) variation.

3.2.1. Nitrogen Dioxide (NO$_2$)

3.2.1.1. Anomalies in NO$_2$ Levels Over the Sub–Region

As presented in the spatial plot in Figure 5a, there was marked reduction in the level of atmospheric nitrogen dioxide over the subregion. Area-averaged annual anomaly shown in Figure 5a is between 0.5×10^{14} and -3×10^{14} cm^{-2} and the mean ($\pm$SD) percentage annual anomaly is $-4.9\% \pm 4.9\%$. The monthly averaged anomalies in NO$_2$ levels are negative from January through September, which coincides with the periods of several restrictions and lockdown in the subregion (see Table 1). The monthly anomalies during the 9-month period lie between 2% and 11% (Figure 5b). With road traffic and other fossil fuel combustion processes being the primary source of atmospheric NO$_2$, this reduction could be attributed to drastic reduction or total stoppage, in some areas, of traffic flow and industrial activities.

3.2.1.2. Anomalies in NO$_2$ Levels Over Epicenters

The nature and level of anomalies over the epicenters varies from one center to the other which is arguably due to the extent, level, and compliance with the restriction and lockdowns. There were also periods of intermittent relaxation of restrictions in some cities that could have influenced the variation of the anomalies. The mean annual anomaly is negative in four of the seven epicenters and ranges between $-1.7\% \pm 13.0\%$ and $-13.9\% \pm 14.0\%$ (see Figure 6). Although the mean annual anomalies are positive in Ashanti Region, Touba, and Abidjan (Figures 6b, 6c, and 6d), there were at least three months with negative anomaly during the period of restrictions in the three epicenters which are indicative of particular times within the several periods of restrictions and lockdowns when
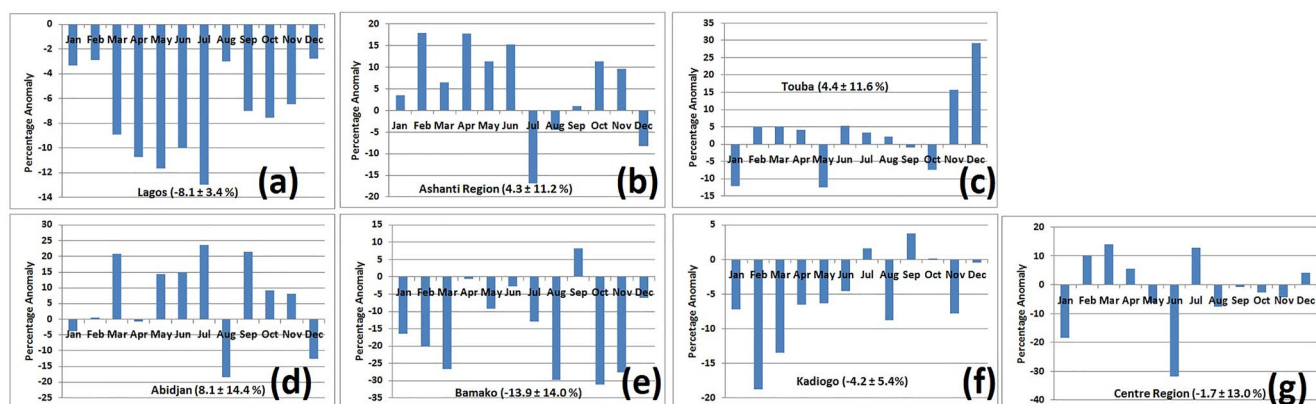
Figure 6. Temporal anomalies of atmospheric NO$_2$ levels over the epicenters. The anomalies for January and February have been excluded from the estimation of the average anomalies for the subregion and the epicenters.

there was the most compliance among the populace. In Touba, for instance, the mean anomaly for the four (4) months with negative anomaly is −8.3% ± 5.4% (Figure 6c).

3.2.2. Carbon Monoxide (CO)

3.2.2.1. Anomalies in CO Levels Over the Subregion

There is a positive annual mean anomaly (1.0 ± 3.2%) in the level of atmospheric CO over the subregion in 2020 relative to the reference years. However, as shown in the spatial plot of the anomaly in level of CO over the subregion (Figure 7a), there is a slight decrease in the annual mean anomaly around the coastal countries in the subregion—Lagos, Abidjan, and Accra which could be attributed to a decrease in the intrusion of transboundary emissions from biomass burning and reduced traffic of vessels and ships at the ports. As presented in Figure 7b, there are some months with negative anomalies in CO levels in the atmosphere in 2020 relative to the reference years. These negative anomalies would be observed on a higher resolution over the epicenters in Section 3.2.2.2. Overall, the restrictions and lockdown did not bring about a decrease in CO levels in the cities but rather an increase that could be due to increased biomass burning, waste/refuse burning, and more domestic cooking using solid fuels rather than eating out during the period of restrictions.

3.2.2.2. Anomalies in CO Levels Over Epicenters

Annual mean anomalies are positive in the epicenters except Abidjan where it is −0.5% ± 6.6% (Figure 8) which implies an increase in atmospheric levels of CO in 2020 relative to the reference years. Even in Abidjan where the anomaly is negative, between the months of March and December while the restriction lasted, there were seven months of positive anomaly (Figure 8d). This shows that there were months of elevated concentrations of atmospheric CO in all the epicenters, including Abidjan during the lockdown period.

3.2.3. Sulfur Dioxide (SO$_2$)

#### 3.2.3.1. Anomalies in SO$_2$ Levels Over the Subregion

But for the area around the Sahelian belt, there is a marked reduction in the level of atmospheric SO$_2$ in the subregion, especially over the cities and urban dwellings (Figure 9a). The decrease in atmospheric levels of SO$_2$ around the cities is similar to the trend observed for NO$_2$, which is expected as both pollutants are majorly from traffic and industrial processes. As shown in Figure 8b, the anomalies are negative in March, April, July, August, September, and December, six of the ten months of restrictions and lockdowns in the region. During these six months, the mean anomaly in atmospheric SO$_2$ level over the subregion is −7.6% ± 10.5%.

#### 3.2.3.2. Anomalies in SO$_2$ Levels Over Epicenters

Across all the epicenters, there is an unequivocal reduction in the levels of atmospheric SO$_2$ between March and December 2020 compared to the reference years. The highest (−17.3% ± 13.9%) and lowest (−2.2% ± 12.8%)
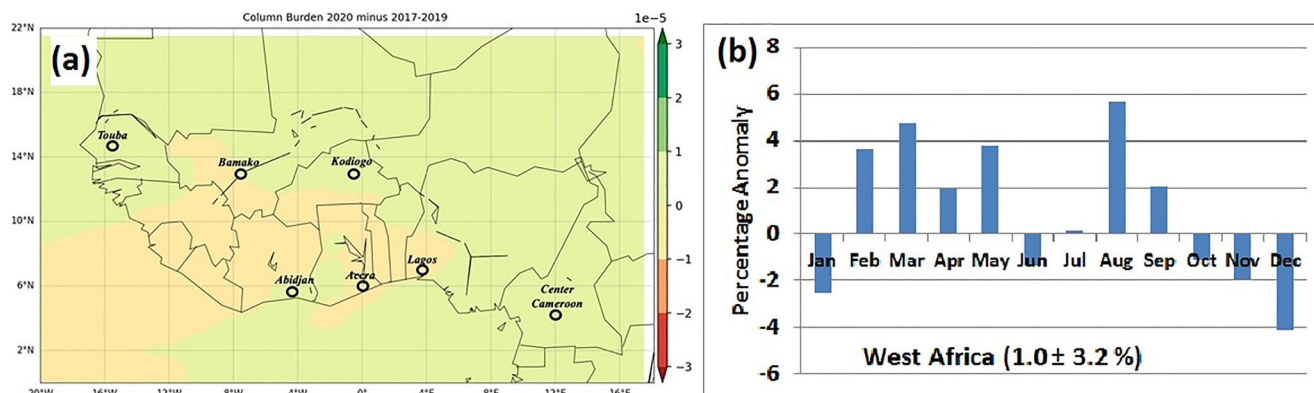
Figure 7. Variation of CO anomaly over the West African subregion (a) spatial variation and (b) temporal (monthly) variation.
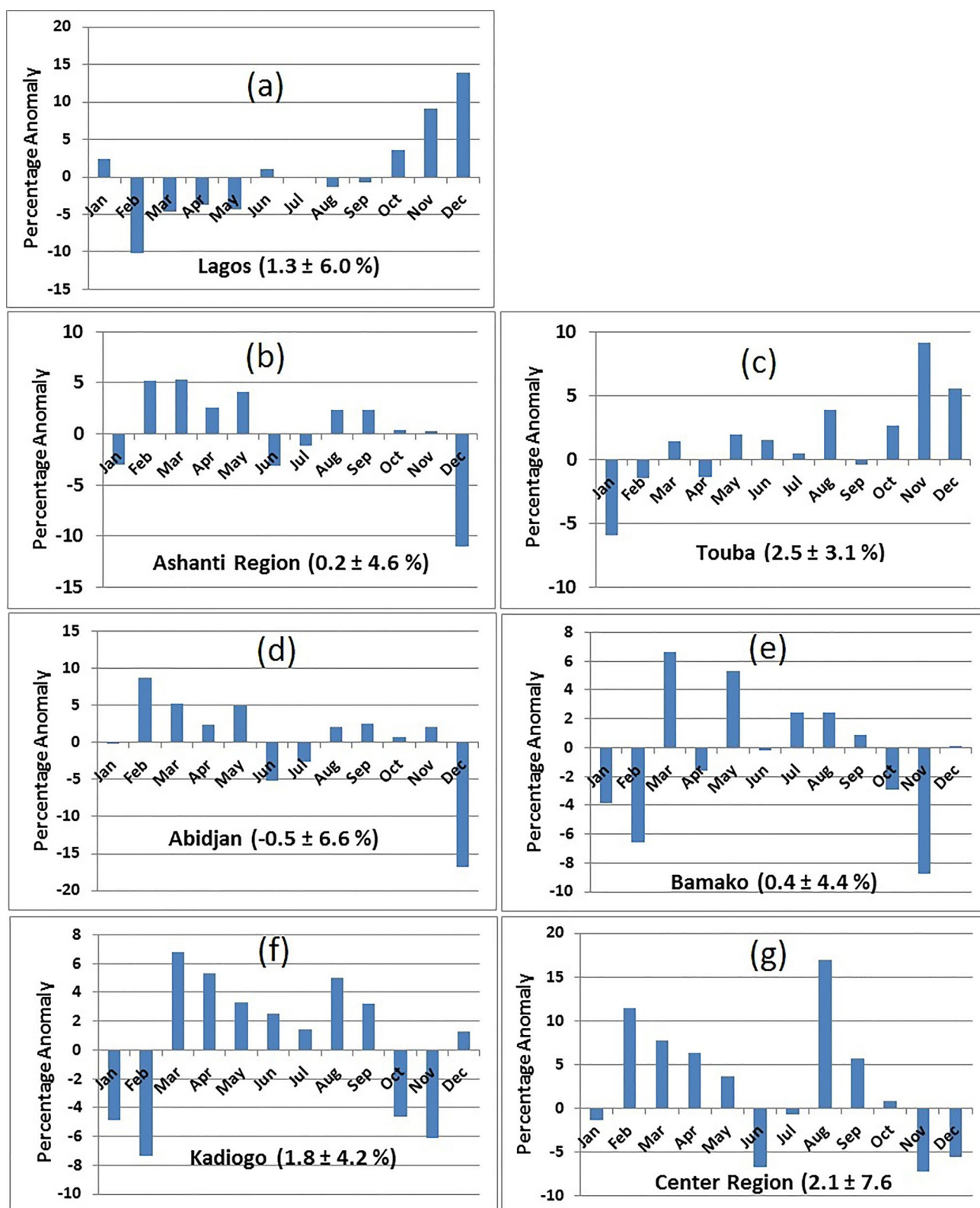
Figure 8. Temporal anomalies of atmospheric CO over the epicenters. The anomalies for January and February have been excluded from the estimation of the average anomalies for the subregion and the epicenters.
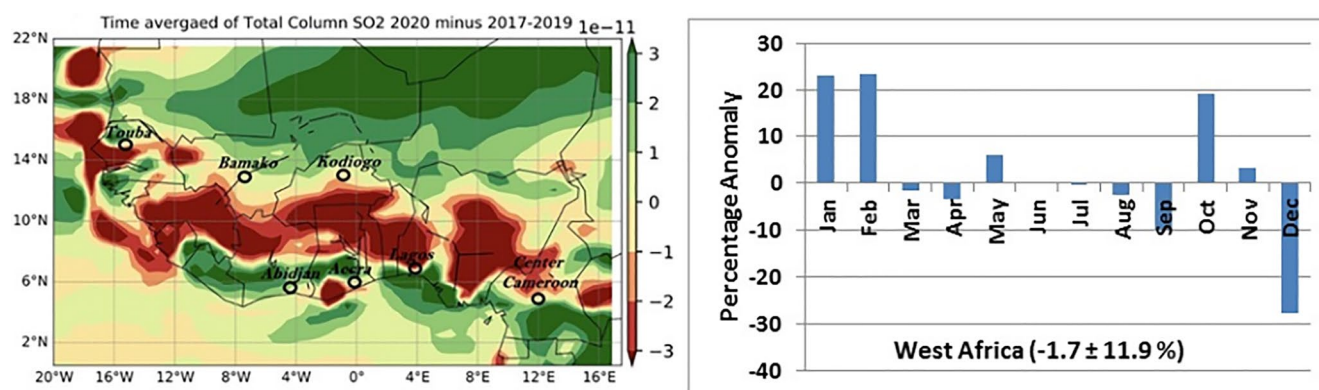
Figure 9. Variation of SO_2 anomaly over the West African subregion (a) spatial variation and (b) temporal (monthly) variation.

reduction were observed in Center Region and Touba, respectively (see Figure 10). The reduction in SO_2 levels are more pronounced during the second waves of the pandemic in all the seven epicenters. This could be due to the fact that there was more compliance with the restriction and lockdown during the second wave of the pandemic. The average anomaly over the seven epicenters during the lockdown periods is $-10.4\% \pm 4.6\%$. This notable and similar trend in the reduction of SO_2 levels over the cities and dwelling areas is attributable to drastic reduction in traffic movement and industrial activities occasioned by the restrictions because SO_2 is a primary pollutant from the combustion of sulfur-containing fossil fuels (Sun et al., 2016).

3.2.4. Ozone (O_3)

Ozone is a secondary pollutant whose level in the atmosphere is significantly impacted by nonlinear chemical interactions between VOCs and NO_X ($NO + NO_2$), a reaction controlled to a large extent by prevailing mesoscale and urban canopy circulation patterns (Marlier et al., 2016; Venter et al., 2020). Ozone titration effect and photochemical ozone formation could significantly affect the level of atmospheric ozone depending on the level of NO_2 and NO available in the atmosphere (Seinfeld & Pandis, 2016).

3.2.4.1. Anomalies in Ozone Levels Over the Subregion

As shown in Figure 11a, across the subregion and over the epicenters, there is a slight increase in the levels of atmospheric ozone. The anomaly in area-averaged ozone levels over the subregion is $1.2\% \pm 1.2\%$ and the trend shows a possible impact of prevailing meteorology on the behavior of atmospheric ozone. The warming caused by the dominance of coarse aerosol cluster (See Section 3.1.2) could have influenced the observed increase in atmospheric ozone. The bimodal peak of the anomaly coincides with the onset and peak of the dry season when ambient temperature is always at the highest annually (see Figure 11b). The anomaly in ozone level over the
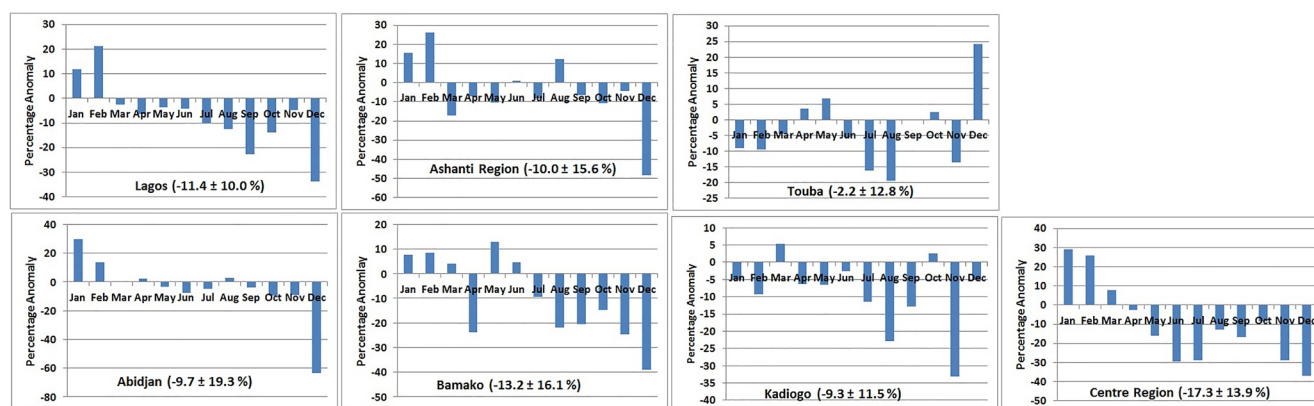
Figure 10. Temporal anomalies of atmospheric SO_2 over the epicenters. The anomalies for January and February have been excluded from the estimation of the average anomalies for the subregion and the epicenters.
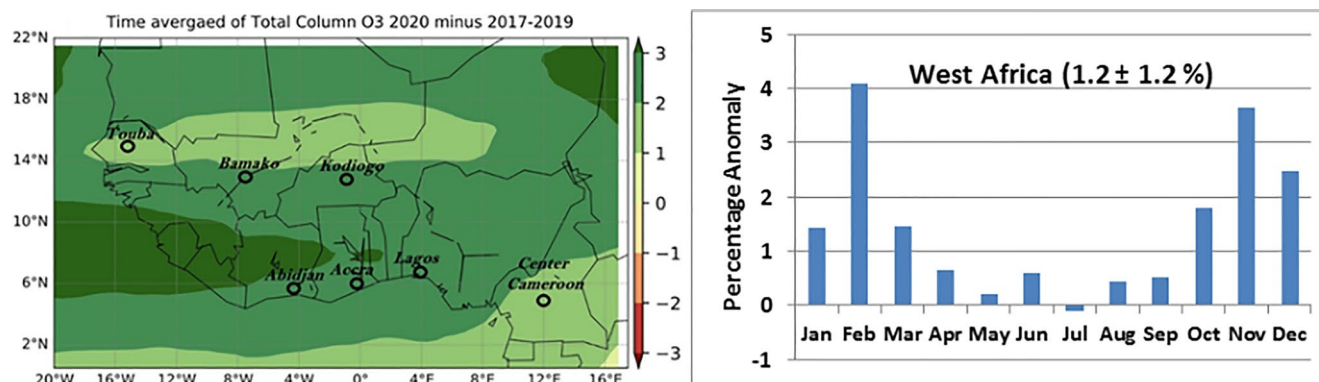
Figure 11. Variation of Ozone anomaly over the West African subregion (a) spatial variation and (b) temporal (monthly) variation.

subregion is low during the West African Monsoon, a period characterized by high precipitation and relatively low ambient temperature.

3.2.4.2. Anomalies in Ozone Levels Over Epicenters

For most of the months of the year, the anomaly is positive in all the seven epicenters indicating an increase in the mean monthly levels of atmospheric ozone in 2020 relative to the reference years (see Figure 12). The magnitude of increase is more for cities further north of the sub-region as against more coastal cities. All of these variations including the bi-modal anomaly discussed in section 3.2.4.1 underpin the possible influence of prevailing meteorology on the anomalies in atmospheric concentration of ozone in 2020 relative to the reference years over the sub-region.

4. Conclusions

The aim of the study was to examine the impact of government restrictions on human and vehicular movement during the COVID-19 pandemic in 2020 on the AQ in selected epicenters in the West African subregion over the subregion. The study resorted to using satellite retrievals and reanalysis due to the nonavailability of reliable long-term ground-based AQ data. Findings from the study reveal that there was significant reduction in atmospheric aerosol (AOD), nitrogen dioxide (NO_2), and sulfur dioxide (SO_2) over the subregion and almost all the epicenters in 2020 compared to the reference years. A remarkable shift in the size distribution of aerosol toward the coarser cluster was also observed. There were slight increases in the atmospheric levels of carbon monoxide and ozone in the same period. The increase in CO levels could be due to increased agricultural burning, waste (domestic and municipal) burning, and increased domestic cooking using solid fuels during the lockdown period
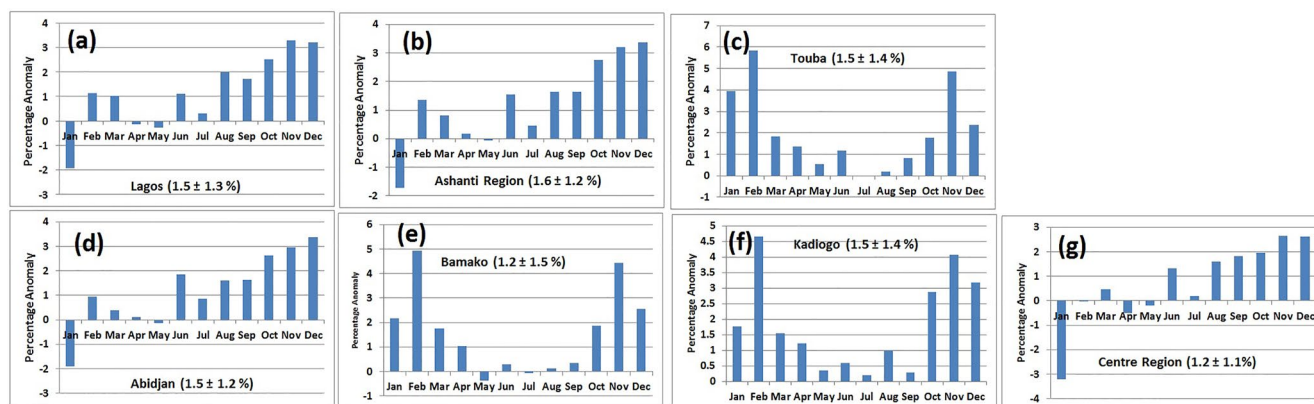
Figure 12. Temporal anomalies of atmospheric ozone over the epicenters. The anomalies for January and February have been excluded from the estimation of the average anomalies for the subregion and the epicenters.

when people were confined to their local residential areas. The anomalies in ozone could be due to a number of factors including meteorology, especially temperature and atmospheric photochemistry. These suggested that although traffic and industrial activities could be the prominent sources of air pollution in the major cities in the subregion, there are other sources that could also contribute significantly to AQ problems. As such, policy makers should realize that a robust AQ management program is needed to significantly improve AQ in these urban areas.

Although most of the findings from this study are in agreement with those obtained in similar studies carried out across most European and US cities, the elevated level of CO observed over the subregion and most of the epicenters is a departure from most of these studies. Although ground-based measurement would be the best approach to assess these unique local CO levels, knowledge of the local terrain suggests that these elevated level of CO could be from domestic waste burning, domestic cooking using solid fuels, and biomass burning from agricultural practices.

Conflict of Interest

The authors declare no conflicts of interest relevant to this study.

Data Availability Statement

The authors acknowledge the data providers, NASA Global Modeling and Assimilation Office, for maintaining Ozone monitoring instrument (OMI) on Aura's satellite and updating the MERRA2 data sets, respectively. Data sets used in this study—MERRA2 (Gelaro et al., 2017) (SO_2, total Angstrom aerosol parameter, CO, and aerosol optical depth (AOD)), OMI (Schoeberl et al., 2006) (Ozone, NO_2, and single scattering albedo), and MODIS (AOD) (Remer et al., 2005)—are all available on the GIOVANNI platform at https://giovanni.gsfc.nasa.gov/giovanni. Most of the data preparation and analyses were done in Microsoft excel using the Pivot Table feature. Statistics and graphical plots/data visualization were carried out in R (version 4.0.3) and MATLAB (R2020a). Raw and processed data set used for the anomalies, temporal analyses (.csv and. xlsx format), and spatial plots of the anomalies (NetCDF) in this study are available at Fawole (2022), "COVID-19: West Africa AQ data," Mendeley Data, V1, https://doi.org/10.17632/3j255ck7yw.1.

References

Andreae, M. O., & Gelencsér, A. (2006). Black carbon or brown carbon? The nature of light-absorbing carbonaceous aerosols. *Atmospheric Chemistry and Physics*, *6*(10), 3131–3148. https://doi.org/10.5194/acp-6-3131-2006

Archer, C. L., Cervone, G., Golbazi, M., Al Fahel, N., & Hultquist, C. (2020). Changes in air quality and human mobility in the USA during the COVID-19 pandemic. *Bulletin of Atmospheric Science and Technology*, *1*(3), 491–514. https://doi.org/10.1007/s42865-020-00019-0

Balis, D., Kroon, M., Koukouli, M., Brinksma, E., Labow, G., Veefkind, J., & McPeters, R. (2007). Validation of Ozone monitoring instrument total ozone column measurements using Brewer and Dobson spectrophotometer ground-based observations. *Journal of Geophysical Research*, *112*(D24), D24S46. https://doi.org/10.1029/2007jd008796

Bauer, S. E., Im, U., Mezuman, K., & Gao, C. Y. (2019). Desert dust, industrialization, and agricultural fires: Health impacts of outdoor air pollution in Africa. *Journal of Geophysical Research: Atmospheres*, *124*(7), 4104–4120. https://doi.org/10.1029/2018jd029336

Bogoch, I. I., Watts, A., Thomas-Bachli, A., Huber, C., Kraemer, M. U., & Khan, K. (2020). Potential for global spread of a novel coronavirus from China. *Journal of Travel Medicine*, *27*(2), taaa011. https://doi.org/10.1093/jtm/taaa011

Boiyo, R., Kumar, K. R., Zhao, T., & Bao, Y. (2017). Climatological analysis of aerosol optical properties over East Africa observed from space-borne sensors during 2001–2015. *Atmospheric Environment*, *152*, 298–313. https://doi.org/10.1016/j.atmosenv.2016.12.050

Bond, T. C., Doherty, S. J., Fahey, D., Forster, P., Berntsen, T., DeAngelo, B., et al. (2013). Bounding the role of black carbon in the climate system: A scientific assessment. *Journal of Geophysical Research: Atmospheres*, *118*(11), 5380–5552. https://doi.org/10.1002/jgrd.50171

Cao, S., Zhang, S., Gao, C., Yan, Y., Bao, J., Su, L., et al. (2021). A long-term analysis of atmospheric black carbon MERRA-2 concentration over China during 1980–2019. *Atmospheric Environment*, *264*, 118662. https://doi.org/10.1016/j.atmosenv.2021.118662

Chen, X., & Yu, B. (2020). First two months of the 2019 coronavirus disease (COVID-19) epidemic in China: Real-time surveillance and evaluation with a second derivative model. *Global health research and policy*, *5*(1), 1–9. https://doi.org/10.1186/s41256-020-00137-4

Choi, J.-O., & Chung, C. E. (2014). Sensitivity of aerosol direct radiative forcing to aerosol vertical profile. *Tellus B: Chemical and Physical Meteorology*, *66*(1), 24376. https://doi.org/10.3402/tellusb.v66.24376

Chung, C. E. (2012). Aerosol direct radiative forcing: A review. In H. Abdul-Razzak (Ed.), *Atmospheric aerosols—regional characteristics—chemistry and physics* (pp. 379–394).

Claquin, T., Schulz, M., & Balkanski, Y. (1999). Modeling the mineralogy of atmospheric dust sources. *Journal of Geophysical Research*, *104*(D18), 22243–22256. https://doi.org/10.1029/1999jd900416

Diop, D., Kama, A., Drame, M. S., Diallo, M., & Niang, D. N. (2018). The use of ALADIN model and MERRA-2 reanalysis to represent dust seasonal dry deposition from 2006 to 2010 in Senegal, West Africa. *Modeling Earth Systems and Environment*, *4*(2), 815–823. https://doi.org/10.1007/s40808-018-0458-5

Dominutti, P., Keita, S., Bahino, J., Colomb, A., Liousse, C., Yoboué, V., et al. (2019). Anthropogenic VOCs in Abidjan, southern west Africa: From source quantification to atmospheric impacts. *Atmospheric Chemistry and Physics*, *19*(18), 11721–11741. https://doi.org/10.5194/acp-19-11721-2019

Eurosurveillance Editorial Team. (2020). Note from the editors: World health organization declares novel coronavirus (2019-nCoV) sixth public health emergency of international concern. *Euro Surveillance*, *25*(5), 200131e. https://doi.org/10.2807/1560-7917.es.2020.25.5.200131e

Fawole, O. G. (2022). COVID-19: West Africa AQ data. Mendeley Data V1. [Dataset]. https://doi.org/10.17632/3j255ck7yw.1

Fawole, O. G., Cai, X., Levine, J. G., Pinker, R. T., & MacKenzie, A. (2016). Detection of a gas flaring signature in the AERONET optical properties of aerosols at a tropical station in West Africa. *Journal of Geophysical Research: Atmospheres*, *121*(24), 14513–14524. https://doi.org/10.1002/2016jd025584

Fayiga, A. O., Ipinmoroti, M. O., & Chirenje, T. (2018). Environmental pollution in Africa. *Environment, Development and Sustainability*, *20*(1), 41–73. https://doi.org/10.1007/s10668-016-9894-4

Filonchyk, M., Hurynovich, V., & Yan, H. (2021). Impact of Covid-19 lockdown on air quality in the Poland, Eastern Europe. *Environmental Research*, *198*, 110454. https://doi.org/10.1016/j.envres.2020.110454

Fu, L., Wang, B., Yuan, T., Chen, X., Ao, Y., Fitzpatrick, T., et al. (2020). Clinical characteristics of coronavirus disease 2019 (COVID-19) in China: A systematic review and meta-analysis. *Journal of Infection*, *80*(6), 656–665. https://doi.org/10.1016/j.jinf.2020.03.041

Fuwape, I., Okpalaonwuka, C., & Ogunjo, S. (2021). Impact of COVID-19 pandemic lockdown on distribution of inorganic pollutants in selected cities of Nigeria. *Air Quality, Atmosphere & Health*, *14*(2), 149–155. https://doi.org/10.1007/s11869-020-00921-8

Gelaro, R., McCarty, W., Suárez, M. J., Todling, R., Molod, A., Takacs, L., et al. (2017). The modern-era retrospective analysis for research and applications, version 2 (MERRA-2). Journal of Climate, *30*(14), 5419–5454. https://doi.org/10.1175/jcli-d-16-0758.1, ([Dataset] Raw data is findable and accessible via. Retrieved from) https://giovanni.gsfc.nasa.gov/giovanni

Hoesly, R. M., Smith, S. J., Feng, L., Klimont, Z., Janssens-Maenhout, G., Pitkanen, T., et al. (2018). Historical (1750–2014) anthropogenic emissions of reactive gases and aerosols from the Community Emissions Data System (CEDS). *Geoscientific Model Development*, *11*(1), 369–408. https://doi.org/10.5194/gmd-11-369-2018

Holloway, T., Levy, H., & Kasibhatla, P. (2000). Global distribution of carbon monoxide. *Journal of Geophysical Research*, *105*(D10), 12123–12147. https://doi.org/10.1029/1999jd901173

Jethva, H., Torres, O., & Ahn, C. (2014). Global assessment of OMI aerosol single-scattering albedo using ground-based AERONET inversion. *Journal of Geophysical Research: Atmospheres*, *119*(14), 9020–9040. https://doi.org/10.1002/2014jd021672

Kaufman, Y. J. (1993). Aerosol optical thickness and atmospheric path radiance. *Journal of Geophysical Research*, *98*(D2), 2677–2692. https://doi.org/10.1029/92jd02427

Lamsal, L. N., Krotkov, N. A., Vasilkov, A., Marchenko, S., Qin, W., Yang, E.-S., et al. (2021). Ozone monitoring instrument (OMI) Aura nitrogen dioxide standard product version 4.0 with improved surface and cloud treatments. *Atmospheric Measurement Techniques*, *14*(1), 455–479. https://doi.org/10.5194/amt-14-455-2021

Lawal, Y. (2021). Africa's low COVID-19 mortality rate: A paradox? *International Journal of Infectious Diseases*, *102*, 118–122. https://doi.org/10.1016/j.ijid.2020.10.038

Levelt, P. F., Hilsenrath, E., Leppelmeier, G. W., van den Oord, G. H., Bhartia, P. K., Tamminen, J., et al. (2006). Science objectives of the ozone monitoring instrument. *IEEE Transactions on Geoscience and Remote Sensing*, *44*(5), 1199–1208. https://doi.org/10.1109/tgrs.2006.872336

Li, Q., Guan, X., Wu, P., Wang, X., Zhou, L., Tong, Y., et al. (2020). Early transmission dynamics in Wuhan, China, of novel coronavirus–infected pneumonia. *New England Journal of Medicine*, *382*(13), 1199–1207. https://doi.org/10.1056/nejmoa2001316

Liousse, C., Assamoi, E., Criqui, P., Granier, C., & Rosset, R. (2014). Explosive growth in African combustion emissions from 2005 to 2030. *Environmental Research Letters*, *9*(3), 035003. https://doi.org/10.1088/1748-9326/9/3/035003

Lourens, A. S., Beukes, J. P., Van Zyl, P. G., Pienaar, J. J., Butler, T. M., Beirle, S., et al. (2012). Re-evaluating the NO_2 hotspot over the South African highveld. *South African Journal of Science*, *108*(11), 1–6. https://doi.org/10.4102/sajs.v108i11/12.1146

Manoharan, V. S., Kotamarthi, R., Feng, Y., & Cadeddu, M. P. (2014). Increased absorption by coarse aerosol particles over the Gangetic–Himalayan region. *Atmospheric Chemistry and Physics*, *14*(3), 1159–1165. https://doi.org/10.5194/acp-14-1159-2014

Marais, E. A., Jacob, D. J., Kurosu, T., Chance, K., Murphy, J., Reeves, C., et al. (2012). Isoprene emissions in Africa inferred from OMI observations of formaldehyde columns. *Atmospheric Chemistry and Physics*, *12*(14), 6219–6235. https://doi.org/10.5194/acp-12-6219-2012

Marlier, M. E., Jina, A. S., Kinney, P. L., & DeFries, R. S. (2016). Extreme air pollution in global megacities. *Current Climate Change Reports*, *2*(1), 15–27. https://doi.org/10.1007/s40641-016-0032-z

Marticorena, B., Chatenet, B., Rajot, J.-L., Traoré, S., Coulibaly, M., Diallo, A., et al. (2010). Temporal variability of mineral dust concentrations over West Africa: Analyses of a pluriannual monitoring from the AMMA Sahelian dust transect. *Atmospheric Chemistry and Physics*, *10*(18), 8899–8915. https://doi.org/10.5194/acp-10-8899-2010

Matthias, V., Quante, M., Arndt, J. A., Badeke, R., Fink, L., Petrik, R., et al. (2021). The role of emission reductions and the meteorological situation for air quality improvements during the COVID-19 lockdown period in central Europe. *Atmospheric Chemistry and Physics*, *21*(18), 13931–13971. https://doi.org/10.5194/acp-21-13931-2021

McPeters, R., & Labow, G. (1996). An assessment of the accuracy of 14.5 years of Nimbus 7 TOMS version 7 ozone data by comparison with the Dobson network. *Geophysical Research Letters*, *23*(25), 3695–3698. https://doi.org/10.1029/96gl03539

Menut, L., Bessagnet, B., Siour, G., Mailler, S., Pennel, R., & Cholakian, A. (2020). Impact of lockdown measures to combat Covid-19 on air quality over Western Europe. *Science of the Total Environment*, *741*, 140426. https://doi.org/10.1016/j.scitotenv.2020.140426

Naidja, L., Ali-Khodja, H., & Khardi, S. (2018). Sources and levels of particulate matter in North African and sub-Saharan cities: A literature review. *Environmental Science and Pollution Research*, *25*(13), 12303–12328. https://doi.org/10.1007/s11356-018-1715-x

Njenga, M. K., Dawa, J., Nanyingi, M., Gachohi, J., Ngere, I., Letko, M., et al. (2020). Why is there low morbidity and mortality of COVID-19 in Africa? *The American Journal of Tropical Medicine and Hygiene*, *103*(2), 564–569. https://doi.org/10.4269/ajtmh.20-0474

Ntoumi, F., & Velavan, T. P. (2021). COVID-19 in Africa: Between hope and reality. *The Lancet Infectious Diseases*, *21*(3), 315. https://doi.org/10.1016/s1473-3099(20)30465-5

O'Neill, N. T., Dubovik, O., & Eck, T. F. (2001). Modified Ångström exponent for the characterization of submicrometer aerosols. *Applied Optics*, *40*(15), 2368–2375. https://doi.org/10.1364/ao.40.002368

Remer, L. A., Kaufman, Y., Tanré, D., Mattoo, S., Chu, D., Martins, J. V., et al. (2005). The MODIS aerosol algorithm, products, and validation. Journal of the Atmospheric Sciences, *62*(4), 947–973. https://doi.org/10.1175/jas3385.1. ([Dataset] Raw data is findable and accessible via. Retrieved from) https://giovanni.gsfc.nasa.gov/giovanni

Rienecker, M. M., Suarez, M. J., Gelaro, R., Todling, R., Bacmeister, J., Liu, E., et al. (2011). MERRA: NASA's modern-era retrospective analysis for research and applications. *Journal of Climate*, *24*(14), 3624–3648. https://doi.org/10.1175/jcli-d-11-00015.1

Rodriguez-Morales, A. J., Bonilla-Aldana, D. K., Tiwari, R., Sah, R., Rabaan, A. A., & Dhama, K. (2020). COVID-19, an emerging coronavirus infection: Current scenario and recent developments-an overview. *Journal of Pure and Applied Microbiology*, *14*(1), 5–12. https://doi.org/10.22207/jpam.14.1.02

Schoeberl, M. R., Douglass, A. R., Hilsenrath, E., Bhartia, P. K., Beer, R., Waters, J. W., et al. (2006). Overview of the EOS Aura mission. *IEEE Transactions on Geoscience and Remote Sensing*, *44*(5), 1066–1074. https://doi.org/10.1109/tgrs.2005.861950. ([Dataset] Raw data is findable and accessible via. Retrieved from) https://giovanni.gsfc.nasa.gov/giovanni

Schwartz, D. A., & Graham, A. L. (2020). Potential maternal and infant outcomes from coronavirus 2019-nCoV (SARS-CoV-2) infecting pregnant women: Lessons from SARS, MERS, and other human coronavirus infections. *Viruses*, *12*(2), 194. https://doi.org/10.3390/v12020194

Seinfeld, J. H., & Pandis, S. N. (2016). *Atmospheric chemistry and physics: From air pollution to climate change*. John Wiley & Sons.

Shikwambana, L. (2019). Long-term observation of global black carbon, organic carbon and smoke using CALIPSO and MERRA-2 data. *Remote Sensing Letters*, *10*(4), 373–380. https://doi.org/10.1080/2150704x.2018.1557789

Shikwambana, L., & Kganyago, M. (2021). Observations of emissions and the influence of meteorological conditions during wildfires: A case study in the USA, Brazil, and Australia during the 2018/19 period. *Atmosphere*, *12*(1), 11. https://doi.org/10.3390/atmos12010011

Spychalski, P., Błażyńska-Spychalska, A., & Kobiela, J. (2020). *Estimating case fatality rates of COVID-19*. The Lancet. Infectious Diseases.

Srivastava, A. K., Bhoyar, P. D., Kanawade, V. P., Devara, P. C., Thomas, A., & Soni, V. K. (2021). Improved air quality during COVID-19 at an urban megacity over the Indo-Gangetic Basin: From stringent to relaxed lockdown phases. *Urban Climate*, *36*, 100791. https://doi.org/10.1016/j.uclim.2021.100791

Stratoulias, D., & Nuthammachot, N. (2020). Air quality development during the COVID-19 pandemic over a medium-sized urban area in Thailand. *Science of the Total Environment*, *746*, 141320. https://doi.org/10.1016/j.scitotenv.2020.141320

Sun, Y., Zwolińska, E., & Chmielewski, A. G. (2016). Abatement technologies for high concentrations of NOx and SO_2 removal from exhaust gases: A review. *Critical Reviews in Environmental Science and Technology*, *46*(2), 119–142. https://doi.org/10.1080/10643389.2015.1063334

Tegen, I., & Lacis, A. A. (1996). Modeling of particle size distribution and its influence on the radiative properties of mineral dust aerosol. *Journal of Geophysical Research*, *101*(D14), 19237–19244. https://doi.org/10.1029/95jd03610

Veefkind, J. P., de Haan, J. F., Brinksma, E. J., Kroon, M., & Levelt, P. F. (2006). Total ozone from the ozone monitoring instrument (OMI) using the DOAS technique. *IEEE Transactions on Geoscience and Remote Sensing*, *44*(5), 1239–1244. https://doi.org/10.1109/tgrs.2006.871204

Venter, Z. S., Aunan, K., Chowdhury, S., & Lelieveld, J. (2020). COVID-19 lockdowns cause global air pollution declines. *Proceedings of the National Academy of Sciences*, *117*(32), 18984–18990. https://doi.org/10.1073/pnas.2006853117

Veselovskii, I., Goloub, P., Podvin, T., Tanre, D., Silva, A. D., Colarco, P., et al. (2018). Characterization of smoke and dust episode over West Africa: Comparison of MERRA-2 modeling with multiwavelength mie–Raman lidar observations. *Atmospheric Measurement Techniques*, *11*(2), 949–969. https://doi.org/10.5194/amt-11-949-2018

Wadvalla, B.-A. (2020). How Africa has tackled COVID-19. *BMJ*, 370. https://doi.org/10.1136/bmj.m2830

Yu, Y., & Chen, P. (2020). Coronavirus disease 2019 (COVID-19) in neonates and children from China: A review. *Frontiers in pediatrics*, *8*, 287. https://doi.org/10.3389/fped.2020.00287

Yusuf, N., Tilmes, S., & Gbobaniyi, E. (2021). Multi-year analysis of aerosol optical properties at various timescales using AERONET data in tropical West Africa. *Journal of Aerosol Science*, *151*, 105625. https://doi.org/10.1016/j.jaerosci.2020.105625